

A fast synthetic iterative scheme for the stationary phonon Boltzmann transport equation

Chuang Zhang^a, Songze Chen^a, Zhaoli Guo^{a,*}, Lei Wu^{b,*}

^aState Key Laboratory of Coal Combustion, Huazhong University of Science and Technology, Wuhan, 430074, China

^bJames Weir Fluids Laboratory, Department of Mechanical and Aerospace Engineering, University of Strathclyde, Glasgow G1 1XJ, UK

Abstract

The heat transfer in solid materials at the micro- and nano-scale can be described by the mesoscopic phonon Boltzmann transport equation (BTE), rather than the macroscopic Fourier's heat conduction equation that works only in the diffusive regime. The implicit discrete ordinate method (DOM) is efficient to find the steady-state solutions of the BTE for highly non-equilibrium heat transfer problems, but converges extremely slowly in the near-diffusive regime. In this paper, a fast synthetic iterative scheme is developed to accelerate convergence for the implicit DOM based on the stationary phonon BTE. The key innovative point of the present scheme is the introduction of the macroscopic synthetic diffusion equation for the temperature, which is obtained from the zero- and first-order moment equations of the phonon BTE. The synthetic diffusion equation, which is asymptotically preserving to the Fourier's heat conduction equation in the diffusive regime, contains a term related to the Fourier's law and a term determined by the second-order moment of the distribution function that reflects the non-Fourier heat transfer. The mesoscopic kinetic equation and macroscopic diffusion equations are tightly coupled together, because the diffusion equation provides the temperature for the BTE, while the BTE provides the high-order moment to the diffusion equation to describe the non-Fourier heat transfer. This synthetic iterative scheme strengthens the coupling of all phonons in the phase space to facilitate the fast convergence from the diffusive to ballistic regimes. Typical numerical tests in one-, two-, and three-dimensional problems demonstrate that our scheme can describe the multiscale heat transfer problems accurately and efficiently. For all test cases convergence is reached within one hundred iteration steps, which is one to three orders of magnitude faster than the traditional implicit DOM in the near-diffusive regime.

Keywords: multiscale heat transfer, phonon Boltzmann transport equation, discrete ordinate method, synthetic scheme

*Corresponding author

Email addresses: zhangcmzt@hust.edu.cn (Chuang Zhang), jacksongze@hust.edu.cn (Songze Chen), zlguo@hust.edu.cn (Zhaoli Guo), lei.wu.100@strath.ac.uk (Lei Wu)

1. INTRODUCTION

The Boltzmann transport equation for heat carriers, including photon, electron, neutron, phonon and so on, is widely used to model multiscale energy transport and conversion [1, 2, 3, 4]. In semiconductor devices, the phonon is regarded as the main heat carrier and the phonon Boltzmann transport equation (BTE) [5, 6, 7] is usually used to predict the multiscale heat transfer in materials [8, 9], while the Fourier’s heat conduction equation is only valid in the diffusive regime, i.e. when the system size is much larger than the phonon mean free path. For steady problems, the phonon BTE is composed of the advection and scattering terms with six degrees of freedom, namely, the physical space (x, y, z coordinates) and the wave vector space (frequency space and solid angle space) [10]. Due to its complicated mathematical expression and multi-variables [11, 2], it is important to numerically solve the phonon BTE efficiently and accurately for actual thermal applications.

Many numerical methods, including the Monte Carlo method [12, 13], discrete ordinate method (DOM) [14], discrete unified gas kinetic scheme (DUGKS) [15, 16], and lattice Boltzmann method (LBM) [17], have been developed to solve the phonon BTE. The Monte Carlo method is the most widely used one in micro/nano scale heat transfer because it can handle with the complex phonon dispersion and scattering physics easily and accurately. However, the requirement that the time step and cell size have to be respectively smaller than the relaxation time and the phonon mean free path restricts its applications in the near-diffusive regime. The Monte Carlo method suffers large statistics errors and converges very slowly in this regime. To fix this problem, some strategies [18, 19, 20] were proposed, such as the energy-based variance-reduced Monte Carlo method [19, 21]. In this method, the stochastic particle description solves only the deviation from the equilibrium state so that it reduces the statistical error significantly and converges faster than the traditional Monte Carlo method when the temperature difference in the simulation domain is small. The DOM employs the deterministic discretization of the wave vector space and physical space, hence it is free of noise. However, the discretization of the six-dimensional non-equilibrium distribution function needs lots of computer memory. Moreover, the phonon advection and scattering are handled separately so that it has large numerical dissipations in the near-diffusive regime, i.e. the numerical heat conductivity is much larger than the physical conductivity. To solve this problem, the DUGKS [15, 16], which couples the phonon scattering and advection together at the cell interface within one time step, has been developed. It works well for all regimes and its time step is not restricted by the relaxation time. The lattice Boltzmann method [22, 23] works well in the near-diffusive regime but it is very hard to capture the multiscale phonon transport physics correctly with a wide range of group velocities and mean free paths, since its use of highly optimized but limited number of discrete solid angles.

For steady heat transfer problems, explicit methods [24, 25] usually converge slowly due to the limitation of the time step by the Courant–Friedrichs–Lewy condition. The implicit iterative scheme, which has no such limitation, will be an excellent choice to find the steady state solution quickly. One of the most popular

implicit methods is the implicit DOM [26, 27, 28, 29]. Given the initial temperature distribution, the phonon BTE for each discretized wave vector is solved iteratively in the whole discretized physical space [30]. After each iteration, the total energy or temperature is updated by the moment of the distribution function over the wave vector space based on the energy conservation of the phonon scattering term. These processes are repeated till convergence. This method converges very fast in the ballistic regime, since the phonon scattering is rare and the information exchange in the physical space is efficient. Note that the energy conservation of the scattering term is not satisfied numerically until the steady state is reached when solving the phonon BTE iteratively for each discretized wave vector [31, 29, 32, 33], which indicates that the coupling of the phonons with different wave vectors are inefficient. Therefore, the iteration converges very slowly in the regimes where the phonon scattering dominates the heat transfer, for example, in the near-diffusive regime. In real materials, unfortunately, the phonon mean free paths span several orders of magnitude [34, 35]. In other words, the phonon BTE is essentially multiscale and for actual thermal engineering, it is necessary to tackle the low efficiency problem in the implicit DOM in the near-diffusive regime.

To accelerate convergence for the implicit DOM in the near-diffusive regime, many strategies [29, 36] have been developed. One of them is the hybrid Fourier-BTE method [30], in which a cutoff Knudsen number is introduced and different equations are used to describe phonon behaviors with different mean free paths. For phonon in each discretized wave vector, if the associated Knudsen number (Kn , the ratio of the mean free path to the characteristic length of the system) is larger than the cutoff one, the traditional implicit DOM is used; otherwise, a modified Fourier equation is used to describe the thermal transport of phonons with small mean free paths. The hybrid Fourier-BTE works well and accelerates convergence in both the ballistic and diffusive regimes. However, the choice of the cutoff Knudsen number that will affect the convergent solution has not been justified rigorously. Different from the explicit numerical treatment of the scattering term in the implicit DOM, the coupled ordinate method (COMET) [31], which was first developed for radiation transport [37], employs the fully implicit treatment on the scattering term in order to numerically ensure the energy conservation of the scattering term. The relationships among the phonon distribution function, equilibrium state and the macroscopic variables are built over the whole wave vector space, and a huge coefficient matrix will be generated and solved iteratively. This method realizes the efficient phonon coupling in both the physical and wave vector spaces and accelerates convergence for all Knudsen numbers. However, it is not easy to solve so many equations with different wave vectors simultaneously.

Another accelerate strategy for the implicit DOM is the synthetic method, which was first proposed for neutron transport [38] and then developed for radiative heat transfer applications [39, 40, 41] and rarefied gas dynamics [42, 43, 44, 45]. The main point of the synthetic scheme [36, 32, 43, 29] is the introduction of the macroscopic moment equations derived from the different moment equations of the BTE, which strengthens the coupling of the heat carriers with different directions or frequencies [41, 36, 29]. Because the mathematical formulas of the phonon BTE under the relaxation time approximation is similar to the radiation

transport equation with isotropic scattering and the Bhatnagar–Gross–Krook (BGK) kinetic model for gas dynamics [1, 2], the synthetic idea will be a good start to find the steady-state solution of the phonon BTE. Recently, an implicit kinetic scheme, which is also a kind of synthetic scheme [38], was developed for multiscale heat transfer problems [33, 46]. The zero-order moment equation of the phonon BTE, namely, the first-law of thermodynamics, is introduced to accelerate convergence for small Knudsen numbers. Because no specific mathematical operator is used to represent the relationship between the heat flux and the temperature at the micro/nano scale, an approximate linear operator with artificial coefficient [47] is constructed to diminish the macroscopic residual. This method works for all Knudsen numbers and accelerates convergence in the near-diffusive regime compared to the implicit DOM. However, the artificial coefficient has to be adjusted to ensure the convergence of the thermal transport in different regimes, as the closer the approximate operator to the real operator, the faster the iteration converges [48, 47],

In this study, a fast synthetic iterative scheme is developed to accelerate convergence for the implicit DOM based on the stationary phonon BTE. Motivated by the synthetic acceleration strategies [32, 36, 38, 42, 43, 44], the zero-order and first-order moment equations of the phonon BTE are combined to derive the diffusion equation for the temperature, which is asymptotically preserving to the Fourier’s heat conduction equation in the diffusive regime. The macroscopic diffusion equation and the phonon BTE are solved sequentially to facilitate the fast convergence to the steady-state solutions. The present scheme can capture the multiscale phonon transport accurately and efficiently, which is easy to implement as it requires few changes to the conventional implicit DOM.

The rest of this article is organized as follows. In Sec. 2, the phonon BTE, the synthetic iterative scheme, and the boundary conditions are introduced and discussed in detail. In Sec. 3, the performances of the present scheme are tested by in a number of one-, two-, and three-dimensional multiscale heat transfer problems. Finally, a conclusion is drawn in Sec. 4.

2. NUMERICAL SCHEME

2.1. Phonon Boltzmann transport equation

For an isotropic wave vector space, the steady-state phonon BTE under the single-mode relaxation time approximation [49, 10] is described by

$$v\mathbf{s} \cdot \nabla f = \frac{f^{eq} - f}{\tau}, \quad (1)$$

where $f(\mathbf{x}, \mathbf{s}, \omega, p)$ is the phonon distribution function in the phase space, \mathbf{x} is the spatial position, \mathbf{s} is the unit direction vector, $v = \partial\omega/\partial k$ is the group velocity, k is the wave vector in one direction, ω is the angular frequency, p is the phonon polarization, τ is the effective relaxation time, and f^{eq} is the equilibrium distribution function given by the Bose-Einstein statistics [6, 4].

For convenience we rewrite the BTE in energy density form,

$$v\mathbf{s} \cdot \nabla e = \frac{e^{eq} - e}{\tau}, \quad (2)$$

by introducing the energy distribution function $e = \hbar\omega D(\omega, p) [f - f^{eq}(T_{\text{ref}})] / 4\pi$ and the associated equilibrium distribution function $e^{eq} = \hbar\omega D(\omega, p) [f^{eq} - f^{eq}(T_{\text{ref}})] / 4\pi$, where \hbar is the Planck's constant divided by 2π , T_{ref} is the reference temperature, and $D(\omega, p) = k^2 / (2\pi^2 v)$ is the phonon density of state.

Assuming the temperature difference in the domain is much smaller than the reference temperature T_{ref} of the system, i.e., $\Delta T \ll T_{\text{ref}}$, then the relaxation time $\tau \approx \tau(\omega, p, T_{\text{ref}})$ is approximately independent of the temperature, and the equilibrium distribution function can be linearized as

$$e^{eq} \approx C(\omega, p, T_{\text{ref}}) \frac{T - T_{\text{ref}}}{4\pi}, \quad (3)$$

where $C(\omega, p, T_{\text{ref}}) = \hbar\omega D(\omega, p) \partial f^{eq} / \partial T$ is the mode specific heat at T_{ref} and T is the temperature [10, 2, 49]. Due to the energy conservation of the scattering term, we have $\sum_p \int_{\omega_{\min,p}}^{\omega_{\max,p}} \int_{4\pi} (e^{eq} - e) / \tau d\Omega d\omega = 0$, where $\omega_{\min,p}$ and $\omega_{\max,p}$ are the minimum and maximum frequency for a given phonon polarization branch p , respectively, and Ω is the solid angle in spherical coordinates. Therefore, the temperature can be obtained by

$$T = T_{\text{ref}} + \left(\sum_p \int_{\omega_{\min,p}}^{\omega_{\max,p}} \int_{4\pi} \frac{e d\Omega}{\tau} d\omega \right) \times \left(\sum_p \int_{\omega_{\min,p}}^{\omega_{\max,p}} \frac{C}{\tau} d\omega \right)^{-1}. \quad (4)$$

The total heat flux is calculated by

$$\mathbf{q} = \sum_p \int_{\omega_{\min,p}}^{\omega_{\max,p}} \int_{4\pi} v s e d\Omega d\omega. \quad (5)$$

Note that from Eq. (2), we can obtain $\nabla \cdot \mathbf{q} = 0$ due to the conservation of the scattering term.

2.2. Phonon dispersion and scattering

In this work, the phonon dispersion curves of the monocrystalline silicon in the [1 0 0] direction are chosen to represent the other directions [50, 35]. Only the acoustic phonon branches, namely, longitude acoustic branch (LA) and transverse acoustic branch (TA), are considered and the dispersion curve reported in [34] is used, i.e.,

$$\omega = c_1 k + c_2 k^2, \quad (6)$$

where $k \in [0, 2\pi/a]$, $a = 0.543\text{nm}$, c_1 and c_2 are two coefficients. For LA, $c_1 = 9.01 \times 10^5 \text{cm/s}$, $c_2 = -2.0 \times 10^{-3} \text{cm}^2/\text{s}$; for TA, $c_1 = 5.23 \times 10^5 \text{cm/s}$, $c_2 = -2.26 \times 10^{-3} \text{cm}^2/\text{s}$ [34]. Apart from above parameters, the phonon scattering [51] is important for the solution of the phonon BTE, too. The Matthiessen's rule is used to couple all phonon scattering mechanisms together [10], i.e.,

$$\tau^{-1} = \tau_{\text{impurity}}^{-1} + \tau_{\text{U}}^{-1} + \tau_{\text{N}}^{-1}, \quad (7)$$

where the specific formulas of impurity scattering τ_{impurity} , U scattering τ_{U} and N scattering τ_{N} can refer to Ref [27].

2.3. Implicit discrete ordinate method

The stationary phonon BTE (2) is usually solved by the implicit DOM [26, 28, 27], in which the frequency space and the solid angle space are discretized into lots of small pieces with certain quadrature rules, respectively. For each phonon branch p , the wave vector k is discretized equally into N_B discrete bands, i.e., $k_b = 2\pi(2b-1)/(2aN_B)$, where $b \in [1, N_B]$. Based on Eq. (6), we can obtain $\omega_b = c_1 k_b + c_2 k_b^2$, $v_{\omega_b, p} = c_1 + 2c_2 k_b$ and $\tau^{-1} = \tau_{\omega_b, p}^{-1}(T_{\text{ref}})$. The mid-point rule is used for the numerical integration of the frequency space. For the solid angle space in spherical coordinates, we set $\mathbf{s} = (\cos \theta, \sin \theta \cos \varphi, \sin \theta \sin \varphi)$, where $\theta \in [0, \pi]$ is the polar angle and $\varphi \in [0, 2\pi]$ is the azimuthal angle. The $\cos \theta \in [-1, 1]$ is discretized with the N_θ -point Gauss-Legendre quadrature [52, 53], while the azimuthal angular space $\varphi \in [0, \pi]$ (due to symmetry) is discretized with the $\frac{N_\varphi}{2}$ -point Gauss-Legendre quadrature. Then we have $N_{dir} = N_\theta \times N_\varphi$ discretized directions \mathbf{s}_α , where $\alpha \in [1, N_{dir}]$.

Giving a macroscopic temperature T^n at the n -th iteration step, the distribution function at the next iteration step e^{n+1} for a given discretized frequency band and direction is updated by solving the following equation

$$e_{\alpha, \omega_b, p}^{n+1} + \tau_{\omega_b, p} v_{\omega_b, p} \mathbf{s}_\alpha \cdot \nabla e_{\alpha, \omega_b, p}^{n+1} = e_{\omega_b, p}^{eq}(T^n). \quad (8)$$

We apply the following finite volume scheme to discretize Eq. (8):

$$e_{i, \alpha, \omega_b, p}^{n+1} + \tau_{\omega_b, p} v_{\omega_b, p} \frac{1}{V_i} \sum_{j \in N(i)} S_{ij} \mathbf{n}_{ij} \cdot \mathbf{s}_\alpha e_{ij, \alpha, \omega_b, p}^{n+1} = e_{i, \omega_b, p}^{eq}(T^n), \quad (9)$$

where V_i is the volume of cell i , $N(i)$ denotes the sets of face neighbor cells of cell i , ij denotes the interface between cell i and cell j , S_{ij} is the area of the interface ij , \mathbf{n}_{ij} is the normal of the interface ij directing from cell i to cell j . The van Leer limiter [54] is used to calculate the distribution function at the cell interface e_{ij} for numerical accuracy and stability. The detailed solution of Eq. (9) can refer to some previous references [55, 56, 26].

Based on Eq. (4), the temperature T^* can be obtained by

$$T^* = T_{\text{ref}} + \left(\sum_p \sum_{b=1}^{N_B} w_b \frac{\sum_{\alpha=1}^{N_{dir}} e_{\alpha, \omega_b, p}^{n+1} w_\alpha}{\tau_{\omega_b, p}} \right) \times \left(\sum_p \sum_{b=1}^{N_B} w_b \frac{C_{\omega_b, p}}{\tau_{\omega_b, p}} \right)^{-1}, \quad (10)$$

where w_b and w_α are the associated weights of discretized frequency space and solid angle space, respectively.

The heat flux is updated by

$$\mathbf{q}^* = \sum_p \sum_{b=1}^{N_B} w_b v_{\omega_b, p} \sum_{\alpha}^{N_{dir}} w_\alpha \mathbf{s}_\alpha e_{\alpha, \omega_b, p}^{n+1}. \quad (11)$$

In the implicit DOM, we set $T^{n+1} = T^*$, $\mathbf{q}^{n+1} = \mathbf{q}^*$. The above process is repeated till convergence.

The implicit DOM converges very fast for the heat transfer in the ballistic regime, however, the number of the iteration steps increases significantly as the system size is much larger than the mean free path of phonons [32, 43, 29, 31, 30]. Our goal in the present work is to develop a fast iterative scheme to accelerate convergence for the implicit DOM in the near-diffusive regime.

2.4. Synthetic diffusion equation for the temperature

One of the reasons for the slow convergence of the traditional iterative scheme (8) is that, at the $(n+1)$ -th iteration step, the temperature is evaluated at the n -th step. To tackle this problem, a macroscopic diffusion equation for the temperature should be established; this equation should be derived exactly from the mesoscopic phonon BTE, meanwhile, it should be able to recover the Fourier's heat transfer law in the diffusive limit.

To do this, let us recall that, when the phonon mean free path is much smaller than the characteristic system size, the Fourier's law is approximately obtained from the first-order Chapman-Enskog expansion [15, 16], where the heat flux is

$$\mathbf{q} \approx \mathbf{q}_{\text{Fourier}} = -k_{\text{bulk}} \nabla T, \quad (12)$$

where

$$k_{\text{bulk}} = \frac{1}{3} \sum_p \int_{\omega_{\min,p}}^{\omega_{\max,p}} C v^2 \tau d\omega \quad (13)$$

is the bulk thermal conductivity obtained in the diffusive limit. Note that k_{bulk} is a constant under the assumption of $\Delta T \ll T_{\text{ref}}$.

When the phonon mean free path is comparable to or even larger than the characteristic system size, high-order contribution to the heat flux emerges, and the heat flux can be separated into the Fourier part and the non-Fourier part:

$$\mathbf{q} = \mathbf{q}_{\text{Fourier}} + \mathbf{q}_{\text{non-Fourier}} = -k_{\text{bulk}} \nabla T + \mathbf{q}_{\text{non-Fourier}}. \quad (14)$$

The key to developing the synthetic diffusion equation is to find the expression for the non-Fourier part of heat flux, so that the diffusion equation for the temperature can be obtained by applying $\nabla \cdot \mathbf{q} = 0$ to Eq. (14), an equation which is exactly the zero-order moment equation of Eq. (2).

To express the heat flux in the form of Eq. (14), the phonon BTE (2) is firstly multiplied by $\tau v \mathbf{s}$ and then integrated over the whole wave vector space, which leads to

$$\sum_p \int_{\omega_{\min,p}}^{\omega_{\max,p}} \int_{4\pi} \tau v^2 \mathbf{s} \mathbf{s} \cdot \nabla e d\Omega d\omega = -\mathbf{q}, \quad (15)$$

$$\nabla \cdot \left(\sum_p \int_{\omega_{\min,p}}^{\omega_{\max,p}} \int_{4\pi} \tau v^2 \mathbf{s} \mathbf{s} \cdot \nabla e d\Omega d\omega \right) = 0. \quad (16)$$

We reformulate Eq. (15) as

$$\sum_p \int_{\omega_{\min,p}}^{\omega_{\max,p}} \int_{4\pi} [\tau v^2 \mathbf{s} \mathbf{s} - A(\omega, p) \mathbf{I}] \cdot \nabla e + A(\omega, p) \mathbf{I} \cdot \nabla e d\Omega d\omega = -\mathbf{q}, \quad (17)$$

where \mathbf{I} is the second order tensor of the unit, while the coefficients are chosen to be

$$A(\omega, p) = k_{\text{bulk}} \left(\tau \sum_p \int_{\omega_{\min,p}}^{\omega_{\max,p}} \frac{C}{\tau} d\omega \right)^{-1}, \quad (18)$$

so that according to Eq. (4) the last term on the left-hand side of Eq. (17) is exactly the Fourier's law:

$$\sum_p \int_{\omega_{min,p}}^{\omega_{max,p}} \int_{4\pi} A(\omega, p) \tau \cdot \nabla \frac{e}{\tau} d\Omega d\omega = k_{\text{bulk}} \nabla T = -\mathbf{q}_{\text{Fourier}}. \quad (19)$$

Clearly, the non-Fourier part of the heat flux is

$$\mathbf{q}_{\text{non-Fourier}} = - \sum_p \int_{\omega_{min,p}}^{\omega_{max,p}} \int_{4\pi} [\tau v^2 \mathbf{s} \mathbf{s} - A(\omega, p) \mathbf{I}] \cdot \nabla e d\Omega d\omega, \quad (20)$$

and the diffusion equation for the temperature is

$$k_{\text{bulk}} \nabla^2 T = \nabla \cdot (\mathbf{q}_{\text{non-Fourier}}). \quad (21)$$

To sum up, we build the correct relationships among these macroscopic variables, i.e., $\mathbf{q}_{\text{non-Fourier}}$, \mathbf{q} and T , by introducing the zero-order and first-order moment equations of the phonon BTE. Equation (21) indicates that the temperature can be calculated by the non-Fourier heat flux. Although the real mathematical formula of the non-Fourier heat flux is unknown, it can be obtained by taking the moment of the distribution function in the framework of phonon BTE according to Eq. (20). In the diffusive limit, $\mathbf{q}_{\text{non-Fourier}} = 0$ and the diffusion equation (21) recovers the traditional Fourier's heat conduction equation correctly.

Next, we will discuss the details of the solution of the macroscopic equation. The finite volume method is used again to solve Eq. (21), i.e.,

$$\sum_{j \in N(i)} S_{ij} \mathbf{n}_{ij} \cdot \nabla T_{ij}^{n+1} = \frac{1}{k_{\text{bulk}}} \sum_{j \in N(i)} S_{ij} \mathbf{n}_{ij} \cdot (\mathbf{q}_{\text{non-Fourier}})_{ij}^*, \quad (22)$$

where $\mathbf{q}_{\text{non-Fourier}}$ is calculated by the second-order moment of the distribution function, i.e.,

$$\begin{aligned} (\mathbf{q}_{\text{non-Fourier}})_{ij}^* &= - \sum_p \int_{\omega_{min,p}}^{\omega_{max,p}} \int_{4\pi} [\tau v^2 \mathbf{s} \mathbf{s} - A(\omega, p) \mathbf{I}] \cdot \nabla e_{ij}^{n+1} d\Omega d\omega \\ &= - \sum_p \sum_{b=1}^{N_B} w_b \sum_{\alpha=1}^{N_{dir}} w_\alpha [\tau_{\omega_b,p} v_{\omega_b,p}^2 \mathbf{s}_\alpha \mathbf{s}_\alpha - A_{\omega_b,p} \mathbf{I}] \cdot \nabla e_{ij,\alpha,\omega_b,p}^{n+1}. \end{aligned} \quad (23)$$

The conjugate gradient method [57, 36, 54] is used to solve the above equation for the update of the temperature and 10 orders of magnitude reduction of residual are enforced.

2.5. Boundary conditions

The boundary condition plays an important role in the heat transfer. Usually, the thermalization boundary condition, specular/diffusely reflecting boundary condition and the periodic boundary condition are considered in the phonon transport [15]. For the distribution function in Eq. (9), detailed treatments of boundary conditions are the same as that in the traditional DOM [27, 58].

Here we focus on the boundary treatments of the macroscopic iteration, i.e., the solution of Eq. (22). Considering a boundary interface ij between the ghost cell j and the inner cell i in Fig. 1, numerical treatments of different boundary conditions are presented as follows:

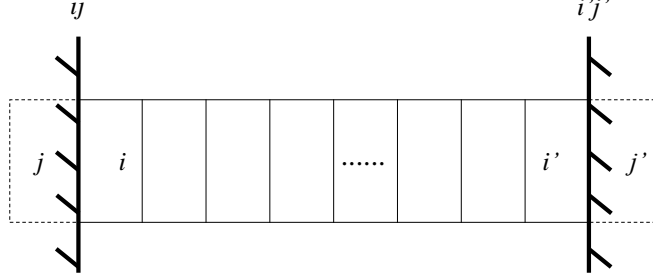


Figure 1: Ghost cells for boundary conditions.

1. The thermalization boundary is a kind of Dirichlet boundary condition with a fixed wall temperature T_w . However, in the non-diffusive regime, there is temperature jump on the boundary, i.e., $T_{ij} \neq T_w$. Based on the moment of the distribution function e_{ij} , i.e., Eq. (10), we can calculate the temperature T_{ij} , then set $T_j = 2T_{ij} - T_i$.
2. The specular/diffusely reflecting boundary condition belongs to the adiabatic boundary condition, which requires that the net heat flux across the boundary is zero, i.e., $\mathbf{n}_{ij} \cdot \mathbf{q}_{ij} = 0$. Thus we have $\mathbf{n}_{ij} \cdot (k_{\text{bulk}} \nabla T_{ij}) = \mathbf{n}_{ij} \cdot \mathbf{q}_{\text{non-Fourier},ij}$, and hence

$$\mathbf{n}_{ij} \cdot \left(k_{\text{bulk}} \frac{T_j - T_i}{\mathbf{x}_j - \mathbf{x}_i} \right) = \mathbf{n}_{ij} \cdot \mathbf{q}_{\text{non-Fourier},ij}. \quad (24)$$

3. The periodic boundary condition usually involves two corresponding boundary interfaces, for example boundary interface ij and its associated interface $i'j'$ between the ghost cell j' and the inner cell i' , as shown in Fig. 1. Two constraints can be derived: $T_{j'} - T_{i'j'} = T_i - T_{ij}$ and $T_j - T_{ij} = T_{i'} - T_{i'j'}$. If there is no temperature difference between the periodic boundaries, i.e., $T_{ij} = T_{i'j'}$, then we have $T_{j'} = T_i$, $T_j = T_{i'}$.

2.6. Solution procedure

In summary, the main procedure of the present synthetic iterative scheme is depicted as follows:

1. give a reasonable macroscopic distribution, i.e., T^n ;
2. update the distribution function at the next iteration step e^{n+1} based on Eq. (9);
3. calculate $\mathbf{q}_{\text{non-Fourier}}$ based on Eq. (23), and update the temperature T^* and the heat flux \mathbf{q}^* based on Eqs. (10) and (11);
4. update the temperature at the next iteration step T^{n+1} based on Eq. (22);
5. if converged, stop the iteration; otherwise, repeat step 2 to step 5.

At the end of each iteration step, the heat flux \mathbf{q}^* and the temperature T^* are regarded as our final results.

In the present synthetic scheme, the macroscopic diffusion equation is introduced to accelerate convergence in the near-diffusive regime and coupled tightly with the phonon BTE. The diffusion equation provides

the temperature for the phonon BTE, while the phonon BTE provides the second-order moment to the diffusion equation to describe the non-Fourier heat transfer. In the diffusion equation (22), the Fourier part heat flux with temperature diffusion and the non-Fourier part heat flux are separated and calculated at two different iteration steps. In the near-diffusive regime, the Fourier-part heat flux dominates the heat transfer and any disturbance of the temperature at one point can be quickly diffused by all other spatial points. While in the ballistic regime, non-Fourier part heat flux dominates the thermal transport and the exchange of information through temperature diffusion is negligible. The combination of the diffusion equation and the implicit DOM makes the present scheme efficient for all regimes.

3. NUMERICAL TESTS

In this section, we present some numerical simulations to assess the accuracy and efficiency of the present scheme for multiscale heat transfer problems. The heat transfer in a 3D cube silicon material with side length L is simulated. In the x , y and z direction, there are left (right), top (bottom), front (back) boundary faces, respectively. The cartesian grids are used to discrete the physical space and N_x , N_y and N_z uniform cells are used for x , y , z direction, respectively. A parameter is introduced to measure the convergence

$$\epsilon = \frac{\sqrt{\sum_i^{N_{cell}} (T_i^n - T_i^{n+1})^2}}{\sqrt{\sum_i^{N_{cell}} (\Delta T \times \Delta T)}}, \quad (25)$$

where $N_{cell} = N_x \times N_y \times N_z$. We assume as $\epsilon < 10^{-8}$ the system is converged. Without special statements, in the following simulations we set $T_{ref} = 300\text{K}$ and the initial temperature distribution in the domain is T_{ref} . At this temperature, the phonon mean free paths of silicon in different frequencies range from tens of nanometers to hundreds of microns. As the characteristic length of the system is a few microns to a few tens of microns, the heat transfer is regarded as in the near-diffusive regime. As $N_B \geq 20$, the numerical integration in the frequency space is regarded as converged based on the calculation of the bulk thermal conductivity, i.e., Eq. (13). In our simulations, $k_{bulk} \approx 145.8\text{W}/(\text{m.K})$. MPI paralleling computation with 24 cores (Intel(R) Xeon(R) CPU E5-2680 v3 @ 2.50GHz) based on the solid angle space is implemented and the CPU time mentioned in the following is the actual wall time for computation.

3.1. One-dimensional case

The quasi-one-dimensional cross-plane heat transfer is tested. A temperature difference ΔT is implemented on the x direction and the temperature of the left and right boundaries are set to be $T_L = T_{ref} + \Delta T/2$ and $T_R = T_{ref} - \Delta T/2$, respectively. Thermalization boundary conditions are used for these two boundaries. The other four boundaries are set to be periodic. Then heat will transfer across the geometry from the left to the right. In order to describe the thermal conduction process in different regimes, we set $N_x = 100$, $N_z = N_y = 1$ and enough discretized directions are used with $N_\theta = 40$ and $N_\varphi = 8$. The phonon dispersion is included with $N_B = 40$, which can capture the multiscale phonon transport physics correctly.

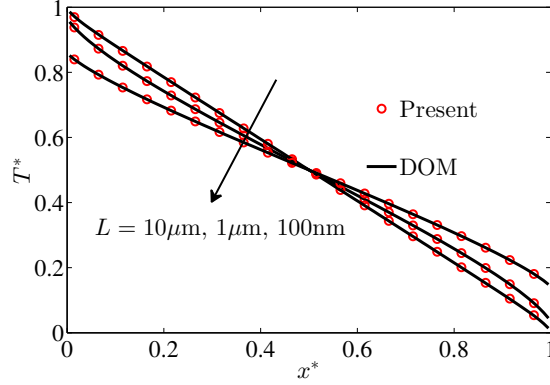


Figure 2: Temperature distributions in the quasi-one-dimensional cross-plane heat transfer with different length L , where $x^* = x/L$ and $T^* = (T - T_R)/\Delta T$. For clarity, results from the present synthetic iterative scheme are shown at every 5 spatial cells.

Table 1: The efficiency of the present scheme in cross-plane heat transfer. Accelerate rate is the ratio of the total CPU time between the implicit DOM and the present scheme. Steps mean the total iteration number. Time per step is the average CPU time cost for each iteration step.

L	Present			DOM			Accelerate rate
	Time (s)	Steps	Time per step	Time (s)	Steps	Time per step	
100 μm	1.24	39	0.0318	>2800	>100000	0.028	> 2258
10 μm	2.26	71	0.0318	329.7	12164	0.0271	145.9
5 μm	2.30	73	0.0315	112.3	4108	0.0273	48.8
1 μm	2.14	67	0.0319	13.3	489	0.0272	6.2
500 nm	2.03	63	0.0322	6.06	220	0.0275	3
100 nm	1.70	53	0.0321	1.58	56	0.0282	0.92

The numerical results are compared with the solutions of the implicit DOM in Fig. 2. It can be observed that the temperature fields predicted by two methods match well with each other at typical length scales. In addition, the efficiency of the present scheme and the implicit DOM is also compared in different length scale, as summarized in Table. 1. It can be found that, compared to the implicit DOM, the present scheme has no acceleration in the ballistic regime. Although the CPU time cost per iteration step by the present scheme increases 15 – 20 percents due to the introduction of the macroscopic iteration, the present scheme accelerates convergence by one to three orders of magnitude in the transition and near-diffusive regimes. As $L \geq 10\mu\text{m}$, it is very difficult for the implicit DOM to reach convergence. However, for the present scheme convergence is reached within 100 iteration steps for all regimes.

3.2. Two-dimensional cases

3.2.1. In-plane heat transfer

In-plane heat transfer is widely simulated in previous works. A constant and small temperature gradient $\Delta T/L$ is applied in the x direction, the temperature of the left and right boundaries are set to be $T_L = T_{\text{ref}} + \Delta T/2$ and $T_R = T_{\text{ref}} - \Delta T/2$, respectively. The top and bottom faces are adiabatic and the others are periodic. The diffusely reflecting boundary conditions are implemented on the adiabatic boundaries. For

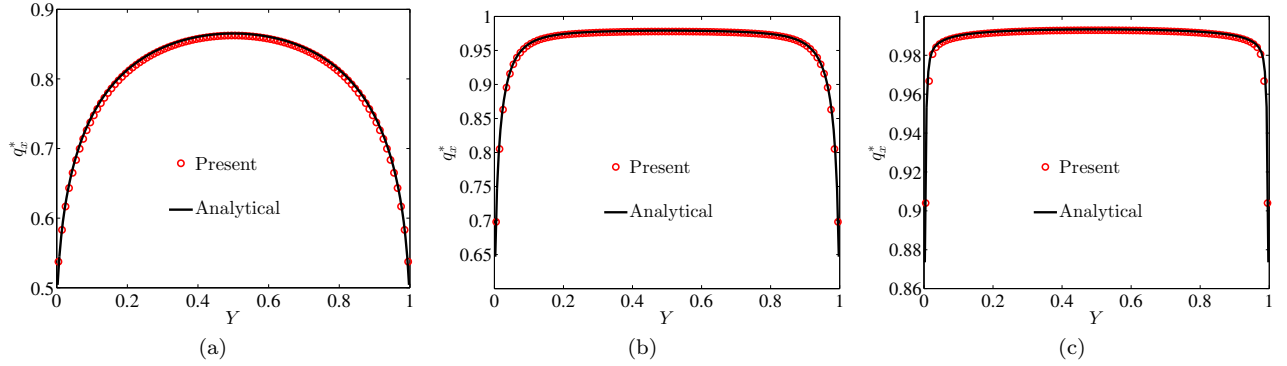


Figure 3: The distribution of in-plane directional heat flux in the y direction. $Y = y/L$, $q_x^* = q_x(Y)/q_{\text{bulk}}$, where $q_{\text{bulk}} = k_{\text{bulk}} \times \Delta T/L$. Red circle is the present numerical results and the black solid line is the analytical solution. (a) $L = 1.0\mu\text{m}$, (b) $L = 10\mu\text{m}$, (c) $L = 100\mu\text{m}$.

the spatial space, we set $N_x = 20$, $N_y = 100$ and $N_z = 1$, which is enough to capture the multiscale heat transfer accurately. The phonon dispersion is included with $N_B = 40$ and $N_\theta \times N_\varphi = 24 \times 24$ discretized directions are used.

The heat flux predicted by the present scheme is compared with the analytical solutions given in Refs. [59, 16]. Numerical results are shown in Fig. 3 and excellent agreements can be observed at different length scales. In addition, the convergence history of the present scheme and implicit DOM is also compared in Fig. 4. As $L = 100\mu\text{m}$, it is not economic to used the implicit DOM, but the present scheme converges very fast. As $L = 10\mu\text{m}$, the CPU time cost by the implicit DOM is 10404 seconds, while CPU time cost of the present scheme is only 67 seconds, which is 155 times faster than the former. Besides, it can be found that the acceleration rate of the present scheme decreases with the decreasing of L , which indicates that the macroscopic diffusion equation loses its function as the Knudsen number increases. In a word, it can be observed that in the near-diffusive regime, the convergence can be reached within 100 steps.

3.2.2. Isothermal solid wall heat transfer

The thermalization boundary conditions are implemented on the left, right, top and bottom faces. The temperature of the left face is fixed at $T_L = T_{\text{ref}} + \Delta T/2$, and the temperature of the other three faces is $T_L = T_{\text{ref}} - \Delta T/2$. The front and back faces are set to be periodic.

The heat transfer with different L is tested in this part. The phonon dispersion is accounted with $N_B = 20$. As $L = 100\text{nm}$, we set $N_x = N_y = 50$, $N_z = 1$, $N_\theta \times N_\varphi = 48 \times 24$ due to the highly non-equilibrium effects and MPI paralleling with 48 cores based on the solid angle space is used to save computation time. For the other cases, the heat transfer comes close to that in the diffusive regime. More cells ($N_x = N_y = 100$, $N_z = 1$) have to be used, while the number of the discretized directions can reduce, for example $N_\theta \times N_\varphi = 24 \times 24$. The numerical results predicted by the present scheme are compared with those obtained by the implicit DOM in Fig. 5. Both the temperature and the heat flux predicted by the present scheme are in excellent agreement with those obtained by the implicit DOM. It can be found that the

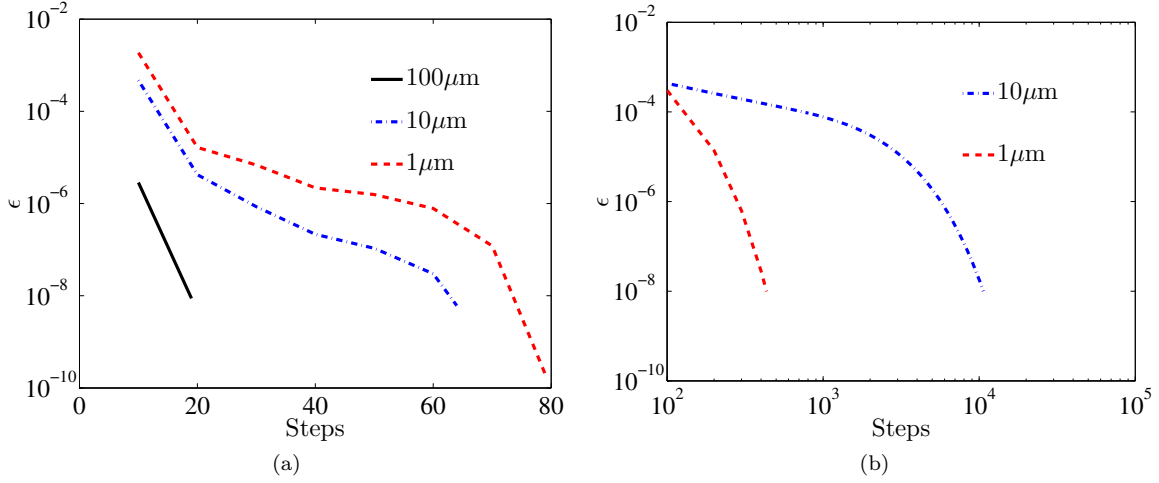


Figure 4: Convergence history of the present scheme and the implicit DOM with different L in the in-plane heat transfer. (a) Present scheme, (b) implicit DOM.

Table 2: The efficiency of the present scheme in isothermal solid wall heat transfer. Accelerate rate is the ratio of the CPU time between the implicit DOM and the present scheme. Steps mean the total iteration number. As $L = 100\text{nm}$, MPI paralleling with 48 cores based on the solid angle space is used.

L	Present		DOM		Accelerate rate
	Time (s)	Steps	Time (s)	Steps	
10 μm	196	72	52931	21840	270
5 μm	199	73	17476	7215	87.8
1 μm	207	75	1917	785	9.3
500 nm	178	65	841	345	4.7
100 nm	416	65	399	66	0.96

temperature jump happens on the left, top and bottom walls as $L = 100\text{nm}$ and $1\mu\text{m}$. As L increases from 100nm to $10\mu\text{m}$, the non-equilibrium thermal effects decrease. The efficiency of the present scheme is tested and shown in Table. 2. As $L = 100\text{nm}$, both the implicit DOM and the present scheme reach convergence within 100 iteration steps. For the implicit DOM, as $L = 1\mu\text{m}$, the convergence speed decreases much, and as $L = 10\mu\text{m}$ it is very hard to reach convergence. But for the present scheme, convergence can be reached within 100 steps for all cases. As L is larger than $1\mu\text{m}$, the present scheme is over ten times faster than the implicit DOM.

3.3. Three-dimensional heat transfer

Based on above subsections, it can be found that the present scheme converges much faster in the near-diffusive regime than the implicit DOM in 1D and 2D cases. To better test the performances of the present scheme in the near-diffusive regime, a large-scale computation of a 3D device-like structure was undertaken [14]. The geometry is shown in Fig. 6. The length of the geometry in the x , y and z direction is L_x , L_y , L_z , respectively. At the center of the top face ($z = 0$), there is a square heating area with side length L_h . The temperature of the heating area is $T_h = T_{\text{ref}} + \Delta T/2$. At the bottom of the geometry ($z = L_z$),

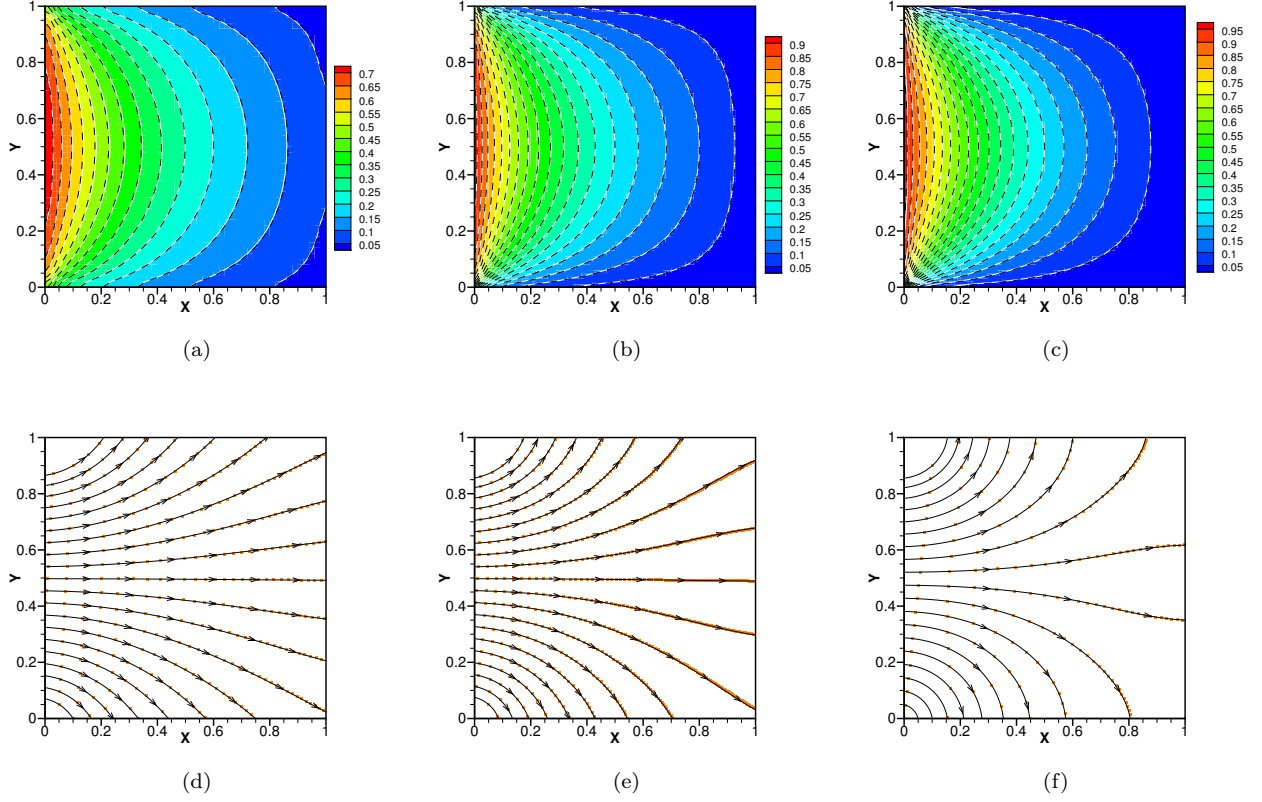


Figure 5: Temperature contour and heat flux line of the isothermal solid wall heat transfer. X, Y are the normalized coordinates, i.e., $X = x/L, Y = y/L$. The normalized temperature is $(T - T_R)/\Delta T$. The above three figures are the temperature field and the bottom are the heat flux streamline. From the left to right are $L = 100\text{nm}, 1\mu\text{m}, 10\mu\text{m}$, respectively. In the temperature contour, colored background with white solid line: implicit DOM; black dash line: present scheme. In the heat flux streamline, black line with arrowhead: implicit DOM; square orange dot: present scheme.

there is a cold area located at the center. The side lengths are L_c and L_y , respectively. The temperature of the cold area is $T_c = T_{\text{ref}} - \Delta T/2$. The other boundaries are all adiabatic. The heat is generated at the top and dissipated at the bottom, which is like the thermal transport mechanism in a transistor.

In order to simulate this problem, the thermalization boundary conditions are implemented on the hot and cold area. For the adiabatic boundaries, the diffusely reflecting boundary conditions are used. We set $L_x = L_y = 2L_z = 4\mu\text{m}, L_h = L_c = 1\mu\text{m}, N_x \times N_y \times N_z = 80 \times 80 \times 40, N_B = 20$ and $N_\theta \times N_\varphi = 24 \times 24$, which is enough to capture the heat transfer process accurately. Due to the large computational amount and memory requirement, we use the MPI paralleling computation with 192 cores based on the solid angle space.

The numerical results including the heat flux streamline and temperature contour are shown in Fig. 7. From a global view (Fig. 7a), the heat flux flows from the hot area to cold area and the temperature decreases gradually along the heat flux line. From the temperature shown in Figs. 7b and 7c, it can be found that there is small temperature jump close to the hot area, which indicates the failure of the Fourier's

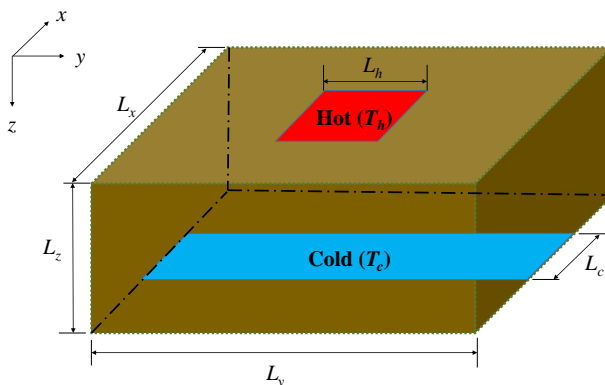


Figure 6: 3D large scale heat transfer.

Table 3: The efficiency of the present scheme in 3D heat transfer, where $N_B = 20$, $L_h = L_c = L_x/4$.

Case	$L_x \times L_y \times L_z$ (μm^3)	$N_x \times N_y \times N_z$	$N_\theta \times N_\varphi$	Steps
1	$1 \times 1 \times 0.5$	$80 \times 80 \times 40$	24×24	99
2	$4 \times 4 \times 2$	$80 \times 80 \times 40$	24×24	72
3	$4 \times 4 \times 4$	$80 \times 80 \times 80$	24×24	77
4	$12 \times 12 \times 6$	$120 \times 120 \times 60$	16×16	67

law. Furthermore, in this simulation, convergence is reached by 72 steps. Other simulations are also done with different numerical settings, as shown in Table. 3. It can be observed that for all cases, convergence is reached within 100 steps in the near-diffusive regime. In summary, the present scheme will be a powerful tool in simulating 3D large scale heat transfer, especially in the near-diffusive regime.

4. CONCLUSIONS

In this work, a synthetic iterative scheme is developed to accelerate convergence for the implicit discrete ordinate method in the near-diffusive regime based on the phonon Boltzmann transport equation. The key point of the present scheme is the introduction of the macroscopic synthetic diffusion equation for the temperature, which is exactly derived from the zero- and first-order moment equations of the phonon BTE and recovers the Fourier's heat conduction equation correctly in the diffusive limit. In the diffusion equation, the heat flux is separated into the Fourier part and the non-Fourier part. The former contains the temperature diffusion information and the latter is obtained by the second-order moment of the distribution function, which captures the non-equilibrium phonon transport physics. The phonon BTE and macroscopic diffusion equations are tightly coupled at two different levels. At the macroscopic level, the diffusion equation provides the temperature for the BTE; at the mesoscopic level, the BTE provides the second-order moment to the diffusion equation to describe the non-Fourier heat transfer. The efficient information exchange strengthens the coupling of all phonons in the phase space and makes the present synthetic scheme converge fast in the simulations of the steady heat transfer problems from diffusive to ballistic regimes.

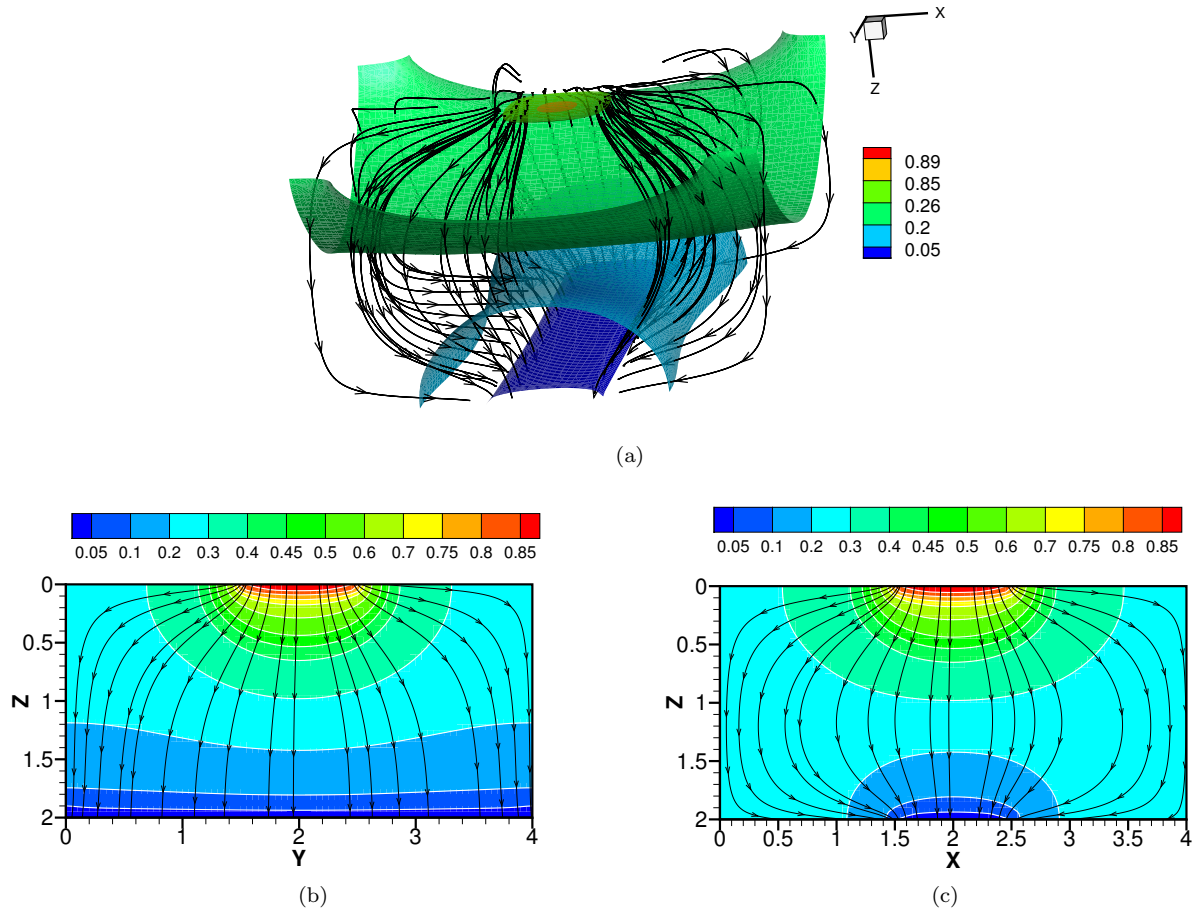


Figure 7: Macroscopic distribution of the 3D heat transfer. Normalized temperature is $(T - T_c)/(T_h - T_c)$, and normalized coordinates are $X = x/L_0$, $Y = y/L_0$, where $L_0 = 1\mu\text{m}$. (a) Temperature iso-surfaces and heat flux streamline, (b) temperature contour and the heat flux streamline at $x = L_x/2$ slice, (c) temperature contour and the heat flux streamline at $y = L_y/2$ slice.

A number of numerical tests have confirmed that the present scheme can predict the thermal transport phenomena accurately in a wide range. Furthermore, the present scheme accelerates convergence significantly in the near-diffusive regime, with about one to three orders of magnitude faster than the conventional implicit DOM. For all cases considered in this study, including one-, two-, and three-dimensional problems, convergence can usually be reached within 100 steps in the near-diffusive regime.

We believe our method can be also used to construct fast convergence scheme for phonon hydrodynamic based on the Callaway's dual relaxation model [60, 61, 28].

Acknowledgments

This work was supported by the National Key Research and Development Plan (No. 2016YFB0600805) and the UK's Engineering and Physical Sciences Research Council (EPSRC) under grant EP/R041938/1.

References

References

- [1] M. Kaviany, Heat Transfer Physics, Cambridge University Press, 2008. doi:10.1017/CB09780511754586.
- [2] G. Chen, Nanoscale energy transport and conversion: a parallel treatment of electrons, molecules, phonons, and photons, Oxford University Press, 2005.
URL <https://global.oup.com/ushe/product/nanoscale-energy-transport-and-conversion-9780195159424?cc=cn&lang=en>
- [3] Z. Zhang, Nano/Microscale Heat Transfer, McGraw Hill professional, McGraw-Hill Education, 2007.
URL <https://books.google.co.jp/books?id=64ygtm0HWtcC>
- [4] N. Laurendeau, Statistical Thermodynamics: Fundamentals and Applications, Cambridge University Press, 2005.
URL <https://books.google.com/books?id=QF6iMewh4KMC>
- [5] A. Majumdar, Microscale energy transport in solids, Taylor and Francis, Washington, DC, 1998.
URL https://books.google.com.hk/books?id=9_8N5k-GsNgC&pg=PA3&lpg=PA3&dq=Microscale+energy+transport+in+solids&source=bl&ots=4vjUHR6KMa&sig=uDIKsvRnBfrP_qxP3r306QjGJDU&hl=zh-CN&sa=X&ved=0ahUKEwil_I2c90jQAhUJkJKKHdv1BJEQ6AEIJTAB#v=onepage&q=Microscale%20energy%20transport%20in%20solids&f=false
- [6] J. M. Ziman, Electrons and phonons: the theory of transport phenomena in solids, Oxford University Press, 1960.
URL <https://global.oup.com/academic/product/electrons-and-phonons-9780198507796?cc=cn&lang=en>
- [7] G. P. Srivastava, The physics of phonons, CRC press, 1990.
URL <https://www.crcpress.com/The-Physics-of-Phonons/Srivastava/p/book/9780852741535>
- [8] D. G. Cahill, W. K. Ford, K. E. Goodson, G. D. Mahan, A. Majumdar, H. J. Maris, R. Merlin, S. R. Phillpot, Nanoscale thermal transport, J. Appl. Phys. 93 (2) (2003) 793–818. doi:10.1063/1.1524305.
URL <http://aip.scitation.org/doi/abs/10.1063/1.1524305>
- [9] D. G. Cahill, P. V. Braun, G. Chen, D. R. Clarke, S. Fan, K. E. Goodson, P. Keblinski, W. P. King, G. D. Mahan, A. Majumdar, et al., Nanoscale thermal transport. ii. 2003–2012, Appl. Phys. Rev. 1 (1) (2014) 011305. doi:10.1063/1.4832615#.
URL <http://aip.scitation.org/doi/full/10.1063/1.4832615#>

- [10] J. Y. Murthy, S. V. J. Narumanchi, J. A. Pascual-Gutierrez, T. Wang, C. Ni, S. R. Mathur, Review of multiscale simulation in submicron heat transfer, *Int. J. Multiscale Computat. Eng.* 3 (1) (2005) 5–32. doi:10.1615/IntJMultCompEng.v3.i1.20.
URL <http://dl.begellhouse.com/journals/61fd1b191cf7e96f,69f10ca36a816eb7,25fd09426d0aaf45.html>
- [11] S. V. Narumanchi, J. Y. Murthy, C. H. Amon, Comparison of different phonon transport models for predicting heat conduction in silicon-on-insulator transistors, *J. Heat Transfer* 127 (7) (2005) 713–723. doi:10.1115/1.1924571.
URL <http://heattransfer.asmedigitalcollection.asme.org/article.aspx?articleid=1447942>
- [12] S. Mazumder, A. Majumdar, Monte carlo study of phonon transport in solid thin films including dispersion and polarization, *J. Heat Transfer* 123 (4) (2001) 749–759. doi:10.1115/1.1377018.
URL <http://dx.doi.org/10.1115/1.1377018>
- [13] S. Mei, L. N. Maurer, Z. Aksamija, I. Knezevic, Full-dispersion monte carlo simulation of phonon transport in micron-sized graphene nanoribbons, *J. Appl. Phys.* 116 (16) (2014) 164307. doi:10.1063/1.4899235.
URL <https://doi.org/10.1063/1.4899235>
- [14] S. A. Ali, G. Kollu, S. Mazumder, P. Sadayappan, A. Mittal, Large-scale parallel computation of the phonon Boltzmann transport equation, *Int. J. Therm. Sci* 86 (2014) 341 – 351. doi:10.1016/j.ijthermalsci.2014.07.019.
URL <http://www.sciencedirect.com/science/article/pii/S1290072914002233>
- [15] Z. Guo, K. Xu, Discrete unified gas kinetic scheme for multiscale heat transfer based on the phonon Boltzmann transport equation, *Int. J. Heat Mass Transfer* 102 (2016) 944 – 958. doi:10.1016/j.ijheatmasstransfer.2016.06.088.
URL <http://www.sciencedirect.com/science/article/pii/S0017931016306731>
- [16] X.-P. Luo, H.-L. Yi, A discrete unified gas kinetic scheme for phonon Boltzmann transport equation accounting for phonon dispersion and polarization, *Int. J. Heat Mass Transfer* 114 (Supplement C) (2017) 970 – 980. doi:10.1016/j.ijheatmasstransfer.2017.06.127.
URL <http://www.sciencedirect.com/science/article/pii/S0017931017302806>
- [17] Y. Guo, M. Wang, Lattice Boltzmann modeling of phonon transport, *J. Comput. Phys.* 315 (2016) 1 – 15. doi:10.1016/j.jcp.2016.03.041.
URL <http://www.sciencedirect.com/science/article/pii/S0021999116001935>

- [18] D. Lacroix, K. Joulain, D. Lemonnier, Monte carlo transient phonon transport in silicon and germanium at nanoscales, *Phys. Rev. B* 72 (2005) 064305. doi:10.1103/PhysRevB.72.064305.
URL <http://link.aps.org/doi/10.1103/PhysRevB.72.064305>
- [19] J.-P. M. Péraud, N. G. Hadjiconstantinou, Efficient simulation of multidimensional phonon transport using energy-based variance-reduced monte carlo formulations, *Phys. Rev. B* 84 (2011) 205331. doi:10.1103/PhysRevB.84.205331.
URL <http://link.aps.org/doi/10.1103/PhysRevB.84.205331>
- [20] J. Randrianalisoa, D. Baillis, Monte carlo simulation of steady-state microscale phonon heat transport, *J. Heat Transfer* 130 (7) (2008) 072404. doi:10.1115/1.2897925.
URL <http://heattransfer.asmedigitalcollection.asme.org/article.aspx?articleid=1449183>
- [21] J.-P. M. Péraud, N. G. Hadjiconstantinou, Adjoint-based deviational monte carlo methods for phonon transport calculations, *Phys. Rev. B* 91 (2015) 235321. doi:10.1103/PhysRevB.91.235321.
URL <https://link.aps.org/doi/10.1103/PhysRevB.91.235321>
- [22] A. Christensen, S. Graham, Multiscale lattice Boltzmann modeling of phonon transport in crystalline semiconductor materials, *Numer. Heat Transfer B* 57 (2) (2010) 89–109. doi:10.1080/10407790903582942.
URL <http://dx.doi.org/10.1080/10407790903582942>
- [23] A. Chattopadhyay, A. Pattamatta, A comparative study of submicron phonon transport using the Boltzmann transport equation and the lattice Boltzmann method, *Numer. Heat Tr. B-fund.* 66 (4) (2014) 360–379. doi:10.1080/10407790.2014.915683.
URL <http://www.tandfonline.com/doi/abs/10.1080/10407790.2014.915683>
- [24] P. Allu, S. Mazumder, Hybrid ballistic–diffusive solution to the frequency-dependent phonon Boltzmann transport equation, *Int. J.Heat Mass Transfer* 100 (Supplement C) (2016) 165 – 177. doi:<https://doi.org/10.1016/j.ijheatmasstransfer.2016.04.049>.
URL <http://www.sciencedirect.com/science/article/pii/S0017931016301430>
- [25] A. J. Minnich, Advances in the measurement and computation of thermal phonon transport properties, *J. Phys-condens. Mat.* 27 (5) (2015) 053202.
URL <http://stacks.iop.org/0953-8984/27/i=5/a=053202>
- [26] T. S. C. W. W. Starnes, K., K. Jayaweera, Numerically stable algorithm for discrete-ordinate-method radiative transfer in multiple scattering and emitting layered media, *Appl. Opt.* 27 (12) (1988) 2502–2509. doi:10.1364/AO.27.002502.
URL <http://ao.osa.org/abstract.cfm?URI=ao-27-12-2502>

- [27] D. Terris, K. Joulain, D. Lemonnier, D. Lacroix, Modeling semiconductor nanostructures thermal properties: The dispersion role, *J. Appl. Phys.* 105 (7) (2009) 073516. doi:10.1063/1.3086409.
URL <http://aip.scitation.org/doi/full/10.1063/1.3086409>
- [28] Y. Guo, M. Wang, Heat transport in two-dimensional materials by directly solving the phonon Boltzmann equation under callaway's dual relaxation model, *Phys. Rev. B* 96 (2017) 134312. doi:10.1103/PhysRevB.96.134312.
URL <https://link.aps.org/doi/10.1103/PhysRevB.96.134312>
- [29] V. A. Fiveland, J. P. Jessee, Acceleration schemes for the discrete ordinates method, *J. Thermophys. Heat Transfer*. 10 (3) (1996) 445–451. doi:10.2514/3.809.
URL <https://arc.aiaa.org/doi/10.2514/3.809>
- [30] J. M. Loy, J. Y. Murthy, D. Singh, A fast hybrid fourier–Boltzmann transport equation solver for nongray phonon transport, *J. Heat Transfer* 135 (1) (2012) 011008–011008. doi:10.1115/1.4007654.
URL <http://dx.doi.org/10.1115/1.4007654>
- [31] S. R. M. Loy, James M., J. Y. Murthy, A coupled ordinates method for convergence acceleration of the phonon Boltzmann transport equation, *J. Heat Transfer* 137 (1) (2015) 012402. doi:10.1115/1.4028806.
URL <http://dx.doi.org/10.1115/1.4028806>
- [32] E. W. Larsen, Diffusion-synthetic acceleration methods for discrete-ordinates problems, *Transport Theor. Stat.* 13 (1-2) (1984) 107–126. doi:10.1080/00411458408211656.
URL <http://dx.doi.org/10.1080/00411458408211656>
- [33] C. Zhang, Z. Guo, S. Chen, Unified implicit kinetic scheme for steady multiscale heat transfer based on the phonon Boltzmann transport equation, *Phys. Rev. E* 96 (2017) 063311. doi:10.1103/PhysRevE.96.063311.
URL <https://link.aps.org/doi/10.1103/PhysRevE.96.063311>
- [34] E. Pop, R. W. Dutton, K. E. Goodson, Analytic band monte carlo model for electron transport in si including acoustic and optical phonon dispersion, *J. Appl. Phys.* 96 (9) (2004) 4998–5005. doi:10.1063/1.1788838.
URL <http://aip.scitation.org/doi/10.1063/1.1788838>
- [35] J. Chung, A. McGaughey, M. Kaviani, Role of phonon dispersion in lattice thermal conductivity modeling, *J. Heat Transfer* 126 (3) (2004) 376–380. doi:10.1115/1.1723469.
URL <http://heattransfer.asmedigitalcollection.asme.org/article.aspx?articleid=1447238>

- [36] M. L. Adams, E. W. Larsen, Fast iterative methods for discrete-ordinates particle transport calculations, *Prog. Nucl. Energ.* 40 (1) (2002) 3 – 159. doi:10.1016/S0149-1970(01)00023-3.
URL <http://www.sciencedirect.com/science/article/pii/S0149197001000233>
- [37] S. R. Mathur, J. Y. Murthy, Coupled ordinates method for multigrid acceleration of radiation calculations, *J. Thermophys. Heat Transfer* 13 (4) (1999) 467–473. doi:10.2514/2.6485.
URL <https://arc.aiaa.org/doi/10.2514/2.6485>
- [38] H. J. Kopp, Synthetic method solution of the transport equation, *Nucl. Sci. Eng.* 17 (1) (1963) 65–74.
arXiv:<https://doi.org/10.13182/NSE63-1>, doi:10.13182/NSE63-1.
URL <https://doi.org/10.13182/NSE63-1>
- [39] E. H. Chui, G. D. Raithby, Implicit solution scheme to improve convergence rate in radiative transfer problems, *Numer. Heat Transf. Part B* 22 (3) (1992) 251–272. doi:10.1080/10407799208944983.
URL <https://doi.org/10.1080/10407799208944983>
- [40] R. E. Alcouffe, Diffusion synthetic acceleration methods for the diamond-differenced discrete-ordinates equations, *Nuclear Science and Engineering* 64 (2) (1977) 344–355. doi:10.13182/NSE77-1.
URL <https://doi.org/10.13182/NSE77-1>
- [41] S. Mazumder, A new numerical procedure for coupling radiation in participating media with other modes of heat transfer, *J. Heat Transfer* 127 (9) (2005) 1037–1045. doi:10.1115/1.1929780.
URL <http://dx.doi.org/10.1115/1.1929780>
- [42] D. Valougeorgis, S. Naris, Acceleration schemes of the discrete velocity method: Gaseous flows in rectangular microchannels, *SIAM J. Sci. Comput.* 25 (2) (2003) 534–552. doi:10.1137/S1064827502406506.
URL <https://doi.org/10.1137/S1064827502406506>
- [43] L. Wu, J. Zhang, H. Liu, Y. Zhang, J. M. Reese, A fast iterative scheme for the linearized Boltzmann equation, *J. Comput. Phys.* 338 (2017) 431 – 451. doi:<https://doi.org/10.1016/j.jcp.2017.03.002>.
URL <http://www.sciencedirect.com/science/article/pii/S0021999117301894>
- [44] W. Su, P. Wang, H. H. Liu, L. Wu, Accurate and efficient computation of the Boltzmann equation for Couette flow: influence of intermolecular potentials on Knudsen layer function and viscous slip coefficient, *J. Comput. Phys.*
- [45] Y. Zhu, C. Zhong, K. Xu, Implicit unified gas-kinetic scheme for steady state solutions in all flow regimes, *J. Comput. Phys.* 315 (2016) 16 – 38. doi:10.1016/j.jcp.2016.03.038.
URL <http://www.sciencedirect.com/science/article/pii/S002199911600190X>
- [46] C. Zhang, Z. Guo, S. Chen.

- [47] R. S. Dembo, S. C. Eisenstat, T. Steihaug, Inexact newton methods, *Siam J. Numer. Anal.* 19 (2) (1982) 400–408. doi:10.1137/0719025.
URL <https://doi.org/10.1137/0719025>
- [48] A. H. Sherman, On newton-iterative methods for the solution of systems of nonlinear equations, *Siam J. Numer. Anal.* 15 (4) (1978) 755–771.
URL <http://www.jstor.org/stable/2156852>
- [49] J.-P. M. Peraud, C. D. Landon, N. G. Hadjiconstantinou, Monte carlo methods for solving the Boltzmann equation, *Annu. Rev. Heat Transfer* 17 205–265. doi:10.1615/AnnualRevHeatTransfer.2014007381.
URL <http://www.dl.begellhouse.com/references/5756967540dd1b03,7deb9f2f1087a9e3,1d883b612ccfafde.html>
- [50] B. N. Brockhouse, Lattice vibrations in silicon and germanium, *Phys. Rev. Lett.* 2 (1959) 256–258. doi:10.1103/PhysRevLett.2.256.
URL <https://link.aps.org/doi/10.1103/PhysRevLett.2.256>
- [51] M. G. Holland, Analysis of lattice thermal conductivity, *Phys. Rev.* 132 (1963) 2461–2471. doi:10.1103/PhysRev.132.2461.
URL <https://link.aps.org/doi/10.1103/PhysRev.132.2461>
- [52] M. Abramowitz, I. Stegun, *Handbook of Mathematical Functions: With Formulas, Graphs, and Mathematical Tables*, Applied mathematics series, Dover Publications, 1964.
URL <https://books.google.co.jp/books?id=MtU8uP7XMvoC>
- [53] N. Hale, A. Townsend, Fast and accurate computation of gauss–legendre and gauss–jacobi quadrature nodes and weights, *Siam J. Sci. Comput* 35 (2) (2013) A652–A674. doi:10.1137/120889873.
URL <http://dx.doi.org/10.1137/120889873>
- [54] E. Süli, D. Mayers, *An Introduction to Numerical Analysis*, Cambridge University Press, 2003.
URL <https://books.google.co.jp/books?id=hj9weaqJTbQC>
- [55] S. Yoon, A. Jameson, Lower-upper symmetric-gauss-seidel method for the euler and navier-stokes equations, *AIAA* 26 (9) (1988) 1025–1026. doi:10.2514/3.10007.
URL <http://arc.aiaa.org/doi/abs/10.2514/3.10007>
- [56] J. Murthy, S. Mathur, Finite volume method for radiative heat transfer using unstructured meshes, *J. Thermophys. Heat Transf.* 12 (3) (1998) 313–321. doi:pdf/10.2514/2.6363.
URL <http://arc.aiaa.org/doi/pdf/10.2514/2.6363>
- [57] B. N. Datta, *Numerical linear algebra and applications*, Siam, 2010.
URL <http://bookstore.siam.org/ot116/>

- [58] T.-Y. Hsieh, H. Lin, T.-J. Hsieh, J.-C. Huang, Thermal conductivity modeling of periodic porous silicon with aligned cylindrical pores, *J. Appl. Phys.* 111 (12) (2012) 124329. doi:10.1063/1.4730962.
URL <http://aip.scitation.org/doi/full/10.1063/1.4730962>
- [59] J. Cuffe, J. K. Eliason, A. A. Maznev, K. C. Collins, J. A. Johnson, A. Shchepetov, M. Prunnila, J. Ahopelto, C. M. Sotomayor Torres, G. Chen, K. A. Nelson, Reconstructing phonon mean-free-path contributions to thermal conductivity using nanoscale membranes, *Phys. Rev. B* 91 (2015) 245423. doi:10.1103/PhysRevB.91.245423.
URL <https://link.aps.org/doi/10.1103/PhysRevB.91.245423>
- [60] S. Lee, D. Broido, K. Esfarjani, G. Chen, Hydrodynamic phonon transport in suspended graphene 6 6290. doi:10.1038/ncomms7290.
- [61] A. Cepellotti, G. Fugallo, L. Paulatto, M. Lazzeri, F. Mauri, N. Marzari, Phonon hydrodynamics in two-dimensional materials 6 (1). doi:10.1038/ncomms7400.
URL <http://www.nature.com/articles/ncomms7400>